Original Article Open Access

Mechanistic Prospective for Human PrP^{C} conversion to PrP^{Sc}: Molecular Dynamic Insights

Nooshin Azari[1], Mohammad Reza Dayer[2,*], Nematollah Razmi[1,3], Mohammad Saaid Dayer[4]

1) Biochemistry Department, Basic Sciences, Fars Science and Research Branch, Islamic Azad University, Shiraz, Islamic Republic of Iran
2) Department of Biology, Faculty of Science, Shahid Chamran University, Ahvaz, Iran
3) Biochemistry Department, Basic Sciences, School of Veterinary Medicine, Shiraz University, Shiraz, Islamic Republic of Iran
4) Department of Parasitology and Medical Entomology, Tarbiat Modares University, Tehran, Islamic Republic of Iran

A B S T R A C T

PrP^{C} conversion to PrP^{Sc} isoform is the main known cause for prion diseases including Crutzfeldt-Jakob, Gerstmann-Sträussler-Sheinker syndrome and fatal familial insomnia in human. The precise mechanism underling this conversion is yet to be well understood. In the present work, using the coordinate file of PrP^{C} (available on the Protein Data Bank) as a starting structure, separate molecular dynamic simulations were carried out at neutral and acidic pH in an explicit water box at 37°C and 1 atmosphere pressure for 10ns second period. Results showed that the acidic pH accelerates PrP^{C} conversion to PrP^{Sc} by decreasing the protein gyration radius, flexibility and protein-solvent hydrogen bonds. In acidic conditions, PrP^{C} attains a more folded and less flexible tertiary structure compared to its native structure at neutral pH; otherwise, the decrease of protein-solvent hydrogen bonds at acidic pH will enhance the hydrophobic character of PrP^{C} that may exhibit association as multimeric assemblies. It can also lower water solubility and increase resistance to proteolytic degradations. Data indicated that there was no sensible protein denaturation during this conversion. It is hypothesized that the formation of slightly misfolded conformations with minor structural changes in secondary and/or tertiary structures are enough to menace scrapie formation in PrP^{C}. Our findings show that scrapie formation seems to be a theoretically reversible process.

Key words: Human Prion Protein, Prion Disease, pH, Misfolded Structure, Molecular Dynamic Simulation

INTRODUCTION

The human prion protein, PrP^{C}, is composed of 253 amino acids encoded by the highly conserved Prnp gene on chromosome 20 [1-3]. This gene is expressed in many tissues such as neurons and immune system cells [4]. PrP^{C} contains two structural domains, a flexible N-terminal domain and a rigid C-terminal domain. The flexible N-terminal domain comprises of residues 1-89, mostly of random coil secondary structure without any regular region, while the rigid C-terminal domain contains residues 90-253, forming three distinct alpha helix and two short anti-parallel beta strands [5, 6]. In the presence of Cu^{+2} or in case of binding to cell membrane, the N-terminal domain of PrP^{C} becomes more structured than when it is present in free isoforms [7-9]. Spectroscopic studies of FTIR and CD indicate that PrP^{C} contains about 43% alpha helix and only 3% beta strand in its secondary structure, with a single disulfide bond between Cys^{179} and Cys^{214} [10-12]. Being the monomeric glycosylated form, the major fraction of PrP^{C} is attached to the extra cellular surface of the plasma membrane by C-terminal residues and through the phosphatidyl inositol component of the membrane phosphoglycerid [11, 13]. Physiologically, PrPC takes part in membrane biological activities such as signal transduction, apoptosis and cell adhesion and so on [14, 15]. Moreover, a small amount of intact PrPC is secreted extracellularly as a soluble protein [16, 17].

One misfolded abnormal isoform of PrP^{C} is known as the scrapie form PrP^{Sc}, in which the beta structure is increased to about 43% at the expense of a decrease in the alpha helix structure to about 30% or less when contrasted to a native PrP^{C}. Unlike a soluble and monomeric isoform of PrP^{C}, the PrP^{Sc} isoform tends to make multimeric aggregates insoluble in water or detergents and increases their resistance to enzymatic proteolysis [18-20]. The formation of such aggregates in tissues and their deposition most often leads to neuronal plaques which are the main cause of prion diseases such as Crutzfeldt-Jacob, Gerstaman-Sträussler-Sheinker syndrome and fatal insomnia in humans [21, 22]. Prion diseases manifest themselves as familial infections or sporadic diseases [22, 23]. According to the Prion-only Hypothesis proposed by Griffith and revised by Lansbury, PrP^{Sc} acts as an infectious pathogen converting PrP^{C} to PrPSc with higher beta structures and increased affinity for polymeric associations [21, 24, 25]. A number of researchers have hypothesized that PrP^{Sc} provides a conformational template, changing infected PrPC to misfolded amyloid aggregates [26-28]. In this model, it is postulated that multimeric associations of PrP^{Sc} are more energetically stable than PrP^{C} monomers and this stability provides a significant driving force for the active infectivity of PrPC by PrPSc [21, 29, 30]. There are reports showing that PrP^{Sc} forms mainly via endocytic pathways and accumulates at high concentrations in the lysosomes of infected cells [27, 31-33]. There are also in vitro and in silico studies showing that acidic pH of lysosomes may trigger the conversion of PrP^{C} to PrP^{Sc} [34-36]. Using molecular dynamic simulations, in the present work we studied the details of a structural alteration phenomenon exerted by acidic pH leading to the effective conversion of PrP^{C} to PrP^{Sc} in a bid to draw a mechanistic logic for this phenomenon.

MATERIALS AND METHODS

The crystal structure of the V210I mutant of human prion protein, PrP^C, in PDB format with PDBID of 2LEJ after initiating I210V mutation was used as a wild-type structure throughout this study. The main reason for choosing this structure was the longest N-terminal tail found in it compared to other structures found on protein data bank resources. This structure is obtained by an X-ray diffraction method and refined at 2Å resolutions [37]. Two copies of this coordinate structure were used separately to simulate neutral and acidic pH effects on the PrP^C structure. Although there are coordinate structures for PrP^C at acidic and neutral pH conditions available on protein data banks, we used two copies of the same coordinate file to simulate PrP^C at neutral and acidic pH after setting the desired pH. As per our experience, starting parallel experiments using the same structures proves to be a useful method to magnify the structural differences in a comparative way. The two structures were each placed in the centre of a rectangular box with dimensions of 6.02×12.15×5.13 nm. The two boxes were filled with SPCE water molecules afterwards so that the proteins were covered by a water shell of 1.0 nm thickness. Molecular dynamic simulations were then performed using a double-precision MPI version of GROMACS 4.5.5 installed on UBUNTU version 12.10 with gromos43a1 force field. Net charges of simulated systems were analyzed by the pre-processor engine of the GROMACS package. System neutralization was done by adding equivalent numbers of chloride ions. Energy minimization was performed for hydrogen atoms, ions, and water molecules in 1500 steps using the steepest descent method to minimize system energy to at least 300kJ/mol. LINCS algorithm was used to apply constraint on bonds lengths. SETTLE algorithm was also used to constrain the geometry of water molecules. The systems were then subjected to a short molecular dynamic with all-bonds restrained for a period of 500 ps before performing full molecular dynamics without any restrains [38]. Molecular dynamic simulations were carried out for 10 ns at 37°C and 1 atmosphere. Berendsen, Thermostat and Barostat, were used for temperature and pressure coupling and Particle Mesh Ewald (PME) method for electrostatic interactions. Time steps of 1 femtosecond were applied to all simulations. Ionized forms of Asp and Glu with negative charges and Arg, and Lys with positive charges were used to set neutral pH, and ionized forms of Arg, His and Lys with positive charges and the rest of the residues with no charges were used to set an acidic pH in our systems [39, 40].

RESULTS

Figure 1 shows the RMSD curve for the N-terminal fragment of residues 85-125 for PrP^C during the simulation period. As indicated, this N-terminal fragment underwent more drastic structural changes in acidic conditions than in neutral pH. Snapshots of the simulated system in Figure 2 reveal that this structural alteration appears to causes this fragment to lay on the globular C-terminal domain, creating an overally round shape for the protein.

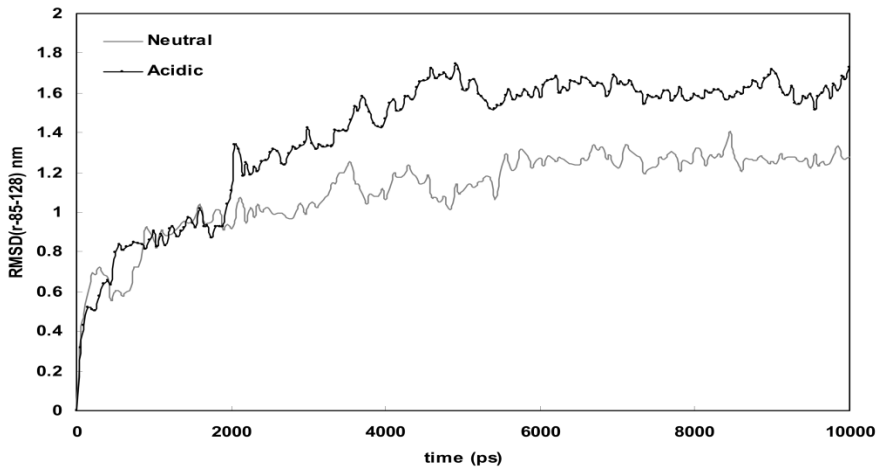

Figure 1: RMSD plot for N-terminal fragment of human prion protein backbone against its initial state obtained from simulations at neutral and acidic pH for 10ns 37^{o}C and 1atomsphere in explicit water box.

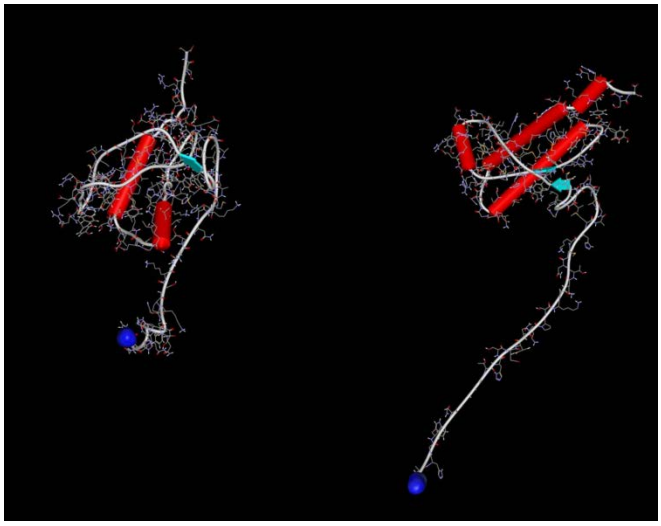

Figure 2: Snapshots showing tertiary structures of prion protein at 100 ps (right) and 10,000 ps (left) frames of simulated system at acidic pH, 37^{o}C and 1atmosphere of pressure.

Figure 3 represents the RMSD curve for the C-terminal domain of residues of 129-231. This curve also shows the higher frequency of structural changes in acidic pH than in neutral pH. Figures 1 and 3 show the same pattern of structural changes, probably caused by the same intervening mechanism as acidic pH. The last phase of RMSD curves (Fig. 1 and 3) at >6000ps conveys the attainment of stability states for acidic and neutral conditions for N and C terminal domains with RMSD fluctuations lower than 2Angstrom. This, in turn, indicates the reliability of results obtained from our simulations.

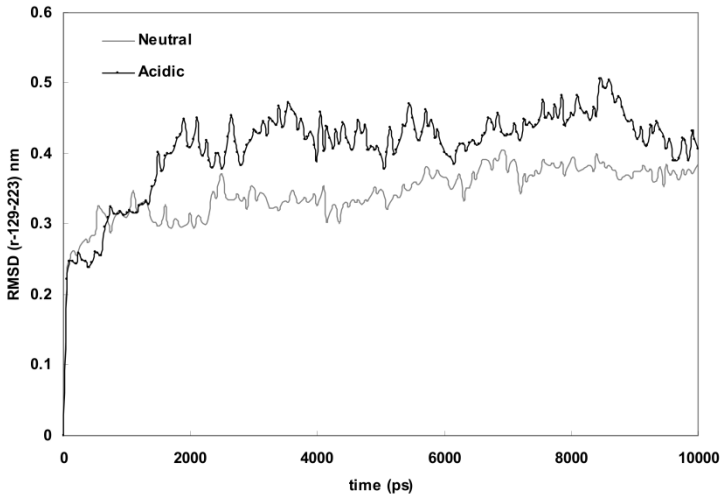

Figure 3: RMSD plot for C-terminal domain of human prion protein backbone against its initial state obtained from simulations at neutral and acidic pH for 10ns 37°C and 1atomsphere in explicit water box.

Figure 4 illustrates the RMSF curve for PrP^C during simulation in acidic and neutral conditions. In this curve, acidifying the protein environment seems to have increased protein flexibility significantly (p-value <0.001). The increase of protein flexibility drives the native protein toward abnormal conformation with suspicious lower solubility and lesser stability when contrasted to the same native protein.

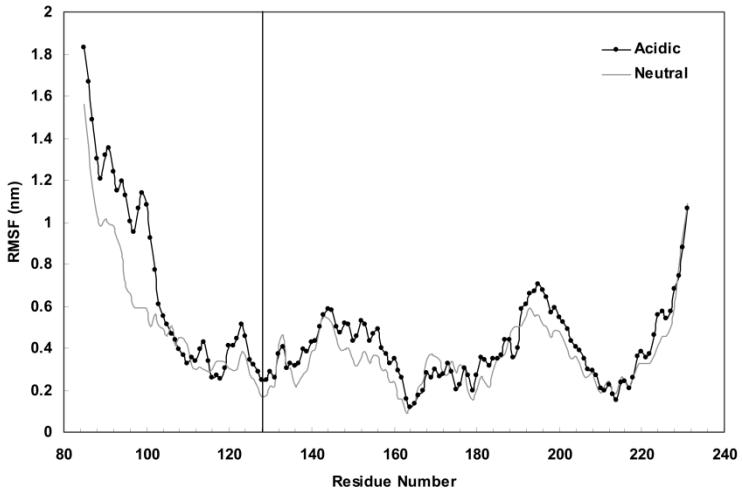

Figure 4: RMSF plot of human prion protein obtained from 10ns simulations at acidic and neutral pH, 37°C and 1atomsphere of pressure in explicit water box.

Figure 5 depicts the gyration radius for N-terminal fragments at acidic and neutral pH. As expected from the trajectory snapshots shown in Figure 2, in acidic pH, the N-terminal fragment moves faster toward the globular C-terminal domain as compared to neutral pH.

This effect causes the formation of a more compact structure with lower gyration radius in acidic pH. Figure 6 shows the same curve for the C-terminal domain. Unlike the N-terminal fragment, the C-terminal domain shows similar compaction status at both pH.

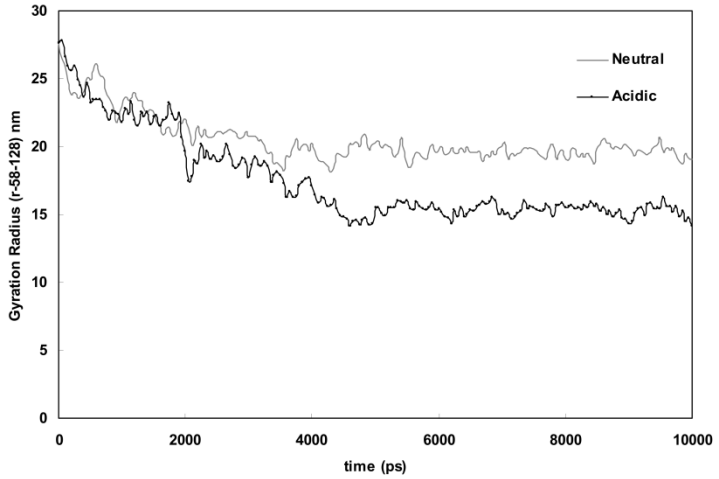

Figure 5: Plot of gyration radius of N-terminal fragment of human prion protein extracted from trajectory files of simulations at neutral and acidic pH, 37^{o}C and 1atomsphere of pressure and in explicit water box.

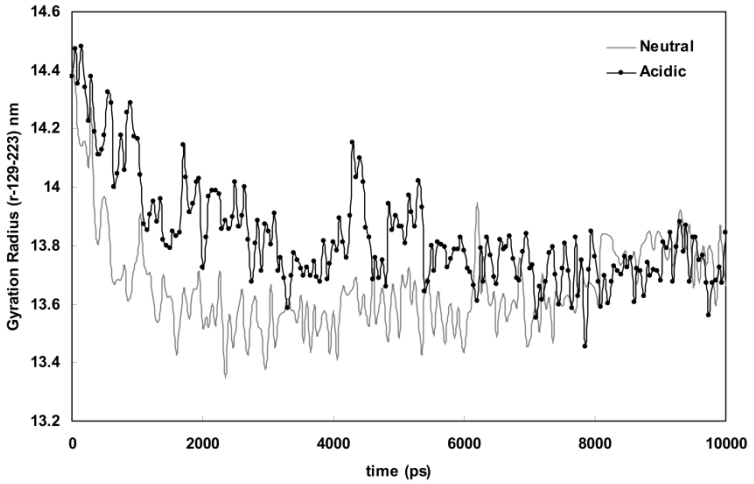

Figure 6: plot of gyration radius of C-terminal domain of human prion protein extracted from trajectory files of simulations at neutral and acidic pH, 37^{o}C and 1atomsphere of pressure and in explicit water box.

The data plotted in Figures 7-9 were obtained from the g-saltbr command of the gromacs package. This command extracted the distance between all probable pairs of polar groups potentially capable of carrying negative or positive charges in a protein including minus-minus, minus-plus and plus-plus with simulation time. Henceforth, the total extracted salt bridges for our systems at neutral and acidic pH are the same. In this context, there are 120, 272 and 136 pairs of salt bridges for minus-minus, plus-minus and plus-plus

charged groups, respectively. In order to make a reasonable comparison, we averaged these distances for minus-minus, plus-minus and plus-plus and depicted them in Figures 7-9. As evident, the distances between these charged groups are in the range of 25-30 Angstrom. Taking into consideration that effective electrostatic interactions take place at a distance of about 3.0 angstrom, and that the energy of electrostatic residues conversely correlates with distance, it seems that these groups are too far away for the electrostatic energy to exert any significant attractive or repulsive force between them. Based on this fact, these averaged distances could be used as indexes for protein compression or decompression in case of any decrease or increase. These curves clearly indicate that the distance between charged groups decreases more significantly at acidic conditions than at neutral pH. This shows the formation of a more compact structure at acidic conditions for PrP^C in which charged groups are brought to near vicinity.

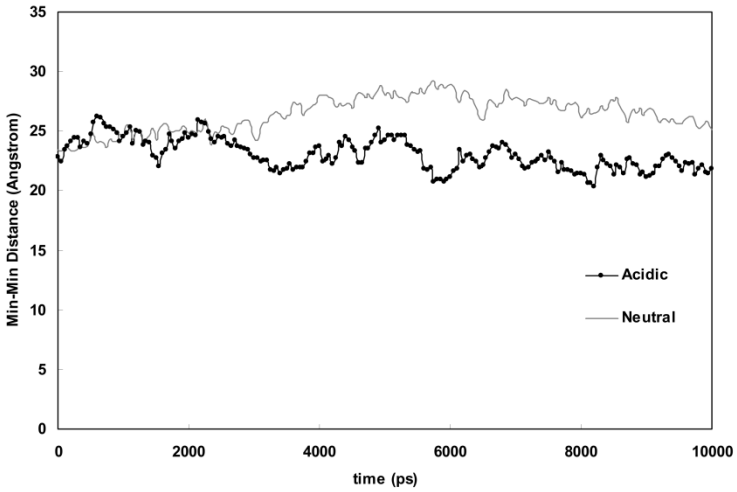

Figure 7: Change in minimum distance between negative-negative (or Minus-Minus) groups of human prion protein at neutral and acidic pH extracted from 10ns simulations at 37^{o}C and 1atomsphere of pressure in explicit water box.

Hydrogen bond counts formed between protein residues in secondary or tertiary structures on the one hand, and between protein residues and surrounding solvents on the other, reflect the structural characteristics of the studied proteins. The alteration of hydrogen bonds during simulation is a useful index to follow up consecutive events leading to protein destabilization. Our data show that human PrP^C in neutral pH exhibits a more hydrated structure, forming an average of 320 hydrogen bonds with solvent molecules, while in acidic pH it forms only 307 hydrogen bonds with the solvent.

Furthermore, protein-protein hydrogen bond calculations reveal that there are 94 hydrogen bonds formed in acidic and 90 in neutral pH. These findings indicate that the

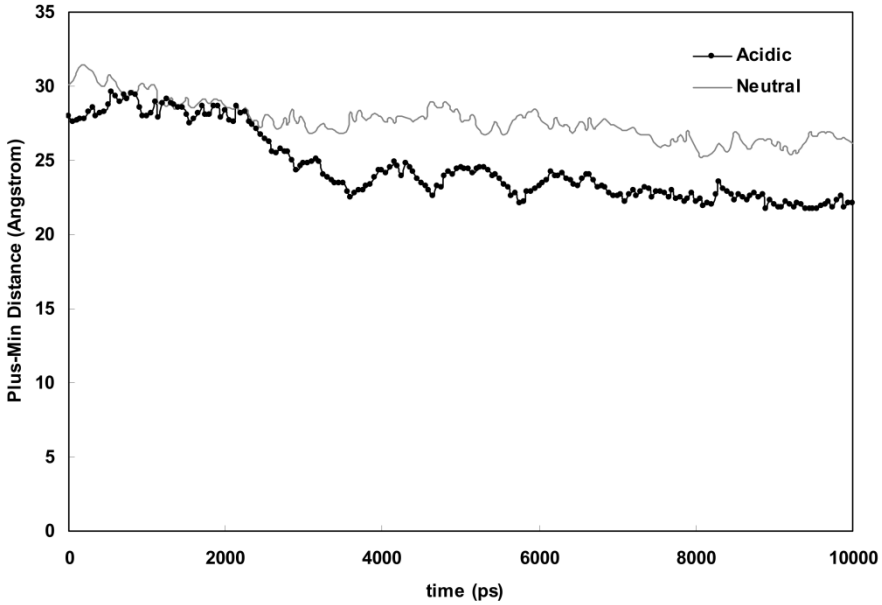

Figure 8: Change in minimum distance between positive-negative (or Plus-Minus) groups of human prion protein at neutral and acidic pH extracted from 10ns simulations at 37^{o}C and 1atomsphere of pressure in explicit water box.

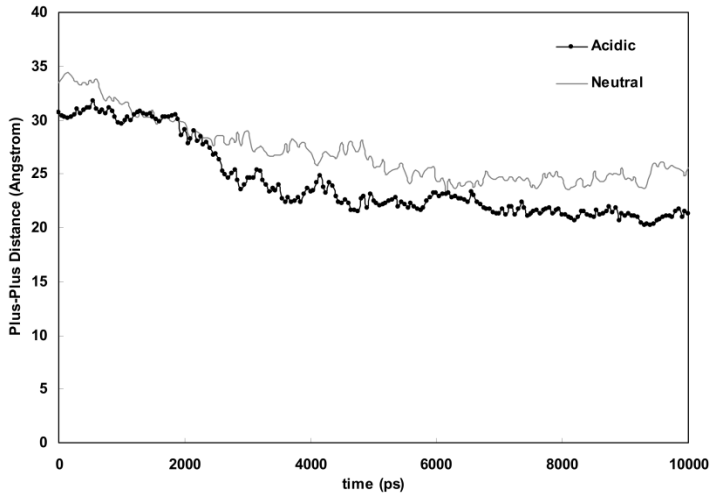

Figure 9: Change in minimum distance between positive-positive (or Plus-Plus) groups of human prion protein at neutral and acidic pH extracted from 10ns simulations at 37^{o}C and 1atomsphere of pressure in explicit water box.

involvements of protein residues in making hydrogen bonds with solvent molecules restrict them from forming extra hydrogen bonds with each other. Therefore, the hydrogen bond between PrP^{C} residues is higher at acidic than neutral pH. This, in turn, means that at acidic pH, PrP^{C} residues most likely prefer to form intramolecular hydrogen bonds instead

of intermolecular ones with solvent molecules. Being in agreement with previous data, the increased intramolecular hydrogen bonds discovered, show an exceptionally more folded state for PrP^C at acidic pH. On the other hand, such tendency in forming hydrogen bonds between protein residues may provide extra forces for protein molecules to collide with each other and join in multimeric aggregates. Structural verifications indicate that PrP^C contains a disulphide bond between Cys^{179} and Cys^{214}. The breakage of intramolecular disulfide bonds and reformation of intermolecular bonds is one of the suspected mechanisms of scrapie formation. To inspect the possibility of the disulfide bond breakage, we calculated the variance of the disulphide bonds' length during the simulation period at both acidic and neutral pH, and used it as an instability index for disulfide bonds. Our data showed a negligible variance in the S-S bond equal to 0.0029% and 0.0027% at acidic and neutral pH respectively. Accordingly, it seems reasonable to conclude that acidic pH does not facilitate disulfide bond breakage during simulation. Figure 10 shows the changes in hydrophobic surface accessible surface (SAS) for PrP^C during simulation at acidic and neutral pH. Clearly, there is no significant difference in SAS propagation with time for different acidic and neutral pHs. The curve implies that no significant denaturation takes place in PrP^C during simulation at acidic pH. In general, structural alterations with notable increases in hydrophobic SAS seem not to be essential for PrP^{Sc} formation.

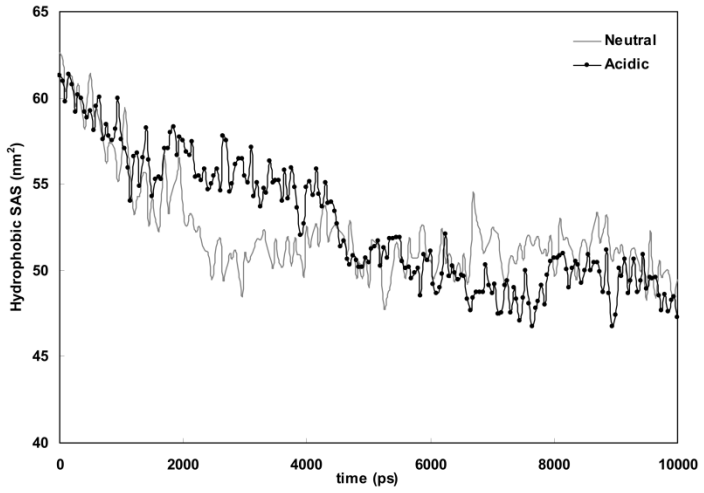

Figure 10: plots of hydrophobic solvent accessible surface (SAS) for human prion protein obtained from simulations at neutral and acidic pH at 37°C and 1atomsphere pressure in explicit water box

Table 1 shows the changes in secondary structures of PrP^C during simulation at acidic and neutral conditions. These data were extracted from PrP^C crystal structures before and after MD simulation and using SPDBV software (http://www.expasy.org/spdbv/). Data indicate the increase in beta structure in acidic pH.

Table 1: Percent of changes in secondary structure of human prion protein at acidic pH in contrast to neutral pH. The data were extracted from trajectory files of simulation for 100 and 10000ps time scales

Secondary structure	% of changes in acidic pH
Alpha Helix	-2%
Beta Strand	+5%
Random Coil	-3%

DISCUSSION

Understanding the transformation mechanism of PrP^{C} to scrapie form is a topic of great interest in molecular medicine research. There are some leading findings to be considered as basic if a more detailed hypothesis is to be constructed in this context. These findings are as follows:

1- Contrary to PrP^{C}, PrP^{Sc} contains more beta and less alpha structures in its secondary structure.
2- Alpha structure seems to be converted to beta structure during the conversion of PrP^{C} to PrP^{Sc}.
3- Unlike PrP^{C}, PrP^{Sc} tends to form multimeric aggregates with lower solubility and increased resistance to proteolysis.
4- In case of prion disease, PrP^{Sc} acts as a conformational template, guiding PrP^{C} to reform its conformation according to PrP^{Sc} conformation.
5- Intramolecular disulfide bond reduction together with the reformation of new intermolecular disulfide bonds is one of the suspected mechanisms for scrapie formation.
6- Acidic pH accelerates PrP^{C} conversion to PrP^{Sc} by inducing structural alteration.

Given these points, we may now discuss our simulation results. The RMSD curve of flexible N-terminal and rigid C-terminal fragments (Fig. 1 and 3) indicate two important points: the first being that the more progression in RMSD plots in acidic pH, the more structural changes happen. The second point is that the progression in N-terminal RMSD plot correlates with that of the C-terminal RMSD plot. This correlation may be interpreted as a causative effect of N-terminal fragment alterations on induction of C-terminal domain events during simulation. The RMSF curve of PrP^{C} at different pH (Fig. 4) shows that the flexibility of PrP^{C} increases significantly at acidic compared to neutral pH, meaning that PrP^{C} accepts a structure of rather different conformation from its native status. The gyration radius of N-terminal and C-terminal domains (Fig. 5 and 6) indicates different structures for PrP^{C} at neutral and acidic pH. The presence of a more folded structure for PrP^{C} at acidic pH can be shown by decreased distances between charged groups on PrP^{C} (Fig. 7-9). The calculation of hydrogen bonds formed between protein residues and solvent molecules indicate significant decrease (4.33%) in protein-solvent hydrogen bonds and significant increase (4.25%) in protein-protein hydrogen bonds (p-value<0.001). This change in hydrogen bond pattern increases the PrP^{C} tendency to form a more compact structure with increased intermolecular hydrogen bonds, leading to protein aggregates of

lower solubility, whereas at neutral pH, PrP^{C} has more hydrated conformation (more protein-solvent hydrogen bonds). As for one of the hypotheses proposed for the conversion of native PrP^{C} to scrapie form of PrP^{Sc}, the infection happens because of the destabilization of the disulphide bond and its following cleavage with the concomitant formation of a new disulphide bond between two prion molecules. This has accounted for the aggregation of prion molecules and PrP^{Sc} formation. However, to examine this hypothesis we calculated the variance in disulfide bond lengths during simulations at neutral and acidic pH. This was to compensate for the shortcoming of molecular dynamic calculations in the simulation and representation of bond breakage and/or bond formation. Our results indicated that there was no significant alteration in the length of disulfide bonds during simulation at both pH (only about 0.002%). Accordingly, we may reject the hypothesis which considers an intervening role for disulfide bonds in PrP^{Sc} formation.

The change in hydrophobic SAS is a useful index which shows the protein folding state during simulation in such as way that its increase with time is considered as an unfolding index. Figure 5 shows that there is no significant change in the SAS curve for the protein during PrP^{C} conversion to PrP^{Sc} in acidic pH. This finding conveys that no protein denaturation is encountered during the formation of a scrapie isoform for prion protein, hence, the conversion may be a reversible process. Finally, our calculations (Table 1) show that upon formation of PrP^{Sc}, beta structure increases about 5% at the expense of a simultaneous decrease in alpha (2%) and random coli (3%) structures.

Based on our results, we can conclude that PrP^{C} conversion to PrP^{Sc} seems to be a reversible process in which monomeric and stable PrP^{C} is converted to multimeric aggregates of decreased solubility. Therefore, the acceleration of scrapie formation at an acidic pH is a result of increased conversion of alpha to beta structures during simulation and formation of intermolecular hydrogen bonds on the one hand, and decreased hydrogen bonds between the protein and solvent on the other, causing monomers of higher affinity to aggregate.

Acknowledgments

The financial support of Shahid Chamran University of Ahvaz and Fars Science & Research Branch, Islamic Azad University, Shiraz, Islamic Republic of Iran are acknowledged.

Conflict of Interest: Authors have no financial or any non-financial competing interests.

REFERENCE

1. Chesebro B, Race R, Wehrly K, Nishio J, Bloom M, Lechner D, Bergstrom S, Robbins K, Mayer L, Keith JM, Garon C, Haase A. Identification of scrapie prion protein-specific mrna in scrapie-infected and uninfected brain. Nature 1985;315:331-333.

2. Basler K, Oesch B, Scott M, Westaway D, Walchli M, Groth DF, McKinley MP, Prusiner SB, Weissmann C. Scrapie and cellular prp isoforms are encoded by the same chromosomal gene. Cell 1986;46:417-428.
3. Sparkes RS, Simon M, Cohn VH, Fournier RE, Lem J, Klisak I, Heinzmann C, Blatt C, Lucero M, Mohandas T, DeArmond SJ, Westaway D, Prusiner SB, Weiner LP. Assignment of the human and mouse prion protein genes to homologous chromosomes. Proc Natl Acad Sci USA 1986;83:7358-7362.
4. Linden R, Martins VR, Prado MA, Cammarota M, Izquierdo I, Brentani RR. Physiology of the prion protein. Physiol Rev 2008;88:673-728.
5. Zahn R, Liu A, Luhrs T, Riek R, von Schroetter C, López García F, Billeter M, Calzolai L, Wide G, Wuthrich K. NMR solution structure of the human prion protein. Proc Natl Acad Sci USA 2000; 97:145–150.
6. Moore RA, Taubner LM, Priola SA. Prion protein misfolding and disease. Curr Opin Struct Biol 2009;19:14-22.
7. Viles JH, Cohen FE, Prusiner SB, Goodin DB, Wright PE, Dyson HJ. Copper binding to the prion protein: structural implications of four identical cooperative binding sites**.** Proc Natl Acad Sci USA 1999;96:2042-2047.
8. Whittal RM, Ball HL, Cohen FE, Burlingame AL, Prusiner SB, Baldwin MA. Copper binding to octarepeat peptides of the prion protein monitored by mass spectrometry. Protein Science 2000; 9:332–343.
9. Morillas M, Swietnicki W, Gambetti P, Surewicz WK. Membrane environment alters the conformational structure of the recombinant human prion protein. J Biol Chem 1999;4:36859-36865.
10. Stahl N, Borchelt DR, Hsiao K, Prusiner SB. Scrapie prion protein contains a phosphatidylinositol glycolipid. Cell 1987;51:229-240.
11. Stahl N, Baldvin MA, Hecker R, Pan KM, Burlingame AL, Prusiner SB. Glycosylinositol phospholipid anchors of the scrapie and cellular prion proteins contain sialic acid. Biochemistry 1992;31:5043-5053.
12. Chen J, Thirumalai D. Helices 2 and 3 are the initiation sites in the $PrP^{C} \rightarrow PrP^{Sc}$ transition. Biochemistry 2013;52:310-319.
13. Mouillet-Richard S, Ermonval M, Chebassier C, Laplanche JL, Lehmann S, Launay JM, Kellermann O. Signal transduction through prion protein. Science 2000;289:1925-1928.
14. Linden R, Cordeiro Y, Lima LM. Allosteric function and dysfunction of the prion protein. Cell Mol Life Sci 2012;69:1105-1124.
15. Gibbings D, Leblanc P, Jay F, Pontier D, Michel F, Schwab, Y, Alais S, Lagrange T, Voinnet O. Human prion protein binds argonaute and promotes accumulation of microrna effector complexes. Nat Struct Mol Biol 2012;19:517-524.
16. Borchelt DR, Rogers M, Stahl N, Telling G, Prusiner SB. Release of the cellular prion protein from cultured cells after loss of its glycoinositol phospholipid anchor. Glycobiology 1993;3:319-329.
17. Starke R, Harrison P, Drummond O, Macgregor I, Mackie I, Machin S. The majority of cellular prion protein released from endothelial cells is soluble. Transfusion 2003;43: 677-678.

18. Meyer RK, McKinley MP, Bowman KA, Braunfeld MB, Barry RA, Prusiner SB. Separation and properties of cellular and scrapie prion proteins. Proc Natl Acad Sci USA 1986;83:2310-2314.
19. Pan KM, Baldwin M, Nguyen J, Gasset M, Serban A, Groth D, Mehlhorn I, Huang Z, Fletterick RJ, Cohen FE, Prusiner SB. Conversion of alpha-helices into beta-sheets features in the formation of the scrapie prion proteins. Proc Natl Acad Sci USA 1993; 90:10962-10966.
20. Stahl N, Baldwin MA, Teplow DB, Hood L, Gibson BW, Burlingame AL, Prusiner SB. Structural studies of the scrapie prion protein using mass spectrometry and amino acid sequencing. Biochemistry 1993;32:1991-2002.
21. Prusiner SB. Prions. Proc Natl Acad Sci USA 1998;95:13363-13383.
22. Prusiner SB, DeArmond SJ. Biology and genetics of prion diseases. Annu Rev Neurosci 1994;17:311-319.
23. DeArmond SJ, Prusiner SB. Etiology and pathogenesis of prion diseases. Am J Pathol 1995;146:785-811.
24. Griffith JS. Self-replication and scrapie. Nature 1967;215:1043-1044.
25. Come JH, Fraser PE, Lansbury PT Jr. A kinetic model for amyloid formation in the prion diseases: importance of seeding. Proc Natl Acad Sci USA 1993;90:5959-5963.
26. Collinge J, Clarke AR. A general model of prion strains and their pathogenicity. Science 2007;318:930-936.
27. Caughey B, Baron GS. Prions and their partners in crime. Nature 2006;443:803-810.
28. Cobb NJ, Surewicz WK. Prion diseases and their biochemical mechanisms. Biochemistry 2009;48:2574-2585.
29. Horiuchi M, Caughey B. Prion protein interconversions and the transmissible spongiform encephalopathies. Structure 1999;7:R231-R240.
30. Tompa P, Tusnady GE, Simon I. The role of dimerization in prion replication. Biophys J 2002; 82:1711–1718
31. Caughey B, Baron GS, Chesebro B, Jeffrey M. Getting a grip on prions: oligomers, amyloids, and pathological membrane interactions. Annu Rev Biochem 2009;78:177-204.
32. Borchelt DR, Taraboulos A, Prusiner SB. Evidence for synthesis of scrapie prion proteins in the endocytic pathway. J Biol Chem 1992;267:16188-16199.
33. Taraboulos A, Serban D, Prusiner SB. Scrapie prion proteins accumulate in the cytoplasm of persistently infected cultured cells. J Cell Biol 1990;110:2117-2132.
34. Zou WQ, Cashman NR. Acidic pH and detergents enhance in vitro conversion of human brain PrPC to PrP^{Sc} -like form. J Biol Chem 2002;277:43492-43947.
35. Calzolai L, Zahn R. Influence of pH on NMR structure and stability of the human prion protein blobular domain. J Biol Chem 2003;278:35592-35596.
36. DeMarco ML, Daggett V. From conversion to aggregation: protoWbril formation of the prion protein. Proc Natl Acad Sci USA 2004;101:2293-2298.
37. Stiffin RM, Sullivan SM, Carlson GM, Holyoak T. Differential inhibition of cytosolic PEPCK by substrate analogues. Kinetic and structural characterization of inhibitor recognition. Biochemistry 2008;47:2099-2109.

38. Lee B, Richards FM. The interpretation of protein structures: estimation of static accessibility. J Mol Biol 1971;55:379-400.
39. Baker WR, Kintanar A. Characterization of the pH titration shifts of ribonuclease A by one- and two-dimensional nuclear magnetic resonance spectroscopy. Arch Biochem Biophys 1996;327:189-199.
40. Peters GH, van Aalten DM, Svendsen A, Bywater R. Essential dynamics of lipase binding sites: the effect of inhibitors of different chain length. Protein Eng 1997;10: 149-158.

Molecular Biology Research Communications 2013;2(4):123-132 MBRC

Original Article Open Access

The Effect of pH on Recombinant C-terminal Domain of Botulinum Neurotoxin Type E (rBoNT/E-HCC)

Seyed Jafar Mousavy[1]*, Mosayeb Rostamian[1], Firouz Ebrahimi[1], Mohammad Reza Dayer[2]

1) Department of Biology, Faculty of Basic Sciences, Imam Hussein University, Tehran, Iran
2) Department of Biology, Faculty of Science, Shahid Chamran University of Ahvaz, Ahvaz, Iran

A B S T R A C T

Recombinant proteins are tending to be the most favorable vaccine-candidates against botulism. Recombinant Carboxy-terminal of botulinum neurotoxin serotype E (rBoNT/E-HCC) has been introduced as an efficient vaccine against botulism type E. In this report, we made an effort to investigate the effect of different pH on protein structure to assess if rBoNT/E-HCC could be used as a vaccine for oral administration. Initially, rBoNT/E-HCC was expressed and purified. Structural changes of rBoNT/E-HCC at several pH conditions were studied by various techniques including circular dichroism (CD), fluorescence, aggregation and UV-Vis spectroscopy. The results showed the more compact and more stable structure for rBoNT/E-HCC at acidic pH, and loosely folded structure at alkaline pH. Our finding as the first step of rBoNT/E-HCC evaluation, hopefully introduce it as a suitable vaccine candidate for oral administration.

Key words: Botulinum Neurotoxin Type E, pH, Fluorescence, Circular Dichroism, Aggregation.

INTRODUCTION

Botulinum neurotoxin is the most potent bacterial protein toxin that is produced by *Clostridium botulinum* [1, 2]. Up to now, seven serotypes of this neurotoxin have been identified and classified using A to G letters [3]. There are several reports indicating that the most important serotypes involving in human botulism are serotype A, B, D and E [4, 5]. The neurotoxins (BoNTs) are synthesized as a single chain precursors with molecular weight of about 150 KDa. The polypeptide chain of neurotoxin is subsequently cleaved by bacterial proteolytic enzymes [6, 7]. This produces a ~50 KDa light chain (LC) fragment from the protein N-terminus and a ~100 KDa heavy chain (HC) fragment from C-terminus [1, 8, 9]. A single disulfide bridge connects these two fragments. HC fragment comprises two functional domains with different functions; an internal domain which is responsible

* Address for correspondence: Department of Biology, Faculty of Basic Sciences, Imam Hussein University, Tehran, Iran.
Fax: +98-2177104935
Tel: +98-2177104934
E-mail: jmosavi@ihu.ac.ir

pISSN 2322-181X eISSN 2345-2005

for toxin translocation to host cells and a C-terminal domain responsible for toxin binding to its receptor. LC fragment is zinc dependent catalytic domain of neurotoxins [10]. Structure flexibility by assistance of several residues of light chain interacted with heavy chain allows LC to be translocated through the membrane channel [11, 12]. LC fragment in host cells hydrolyzes cellular SNARE (soluble N-ethylmaleimide–sensitive fusion protein attachment protein receptor) proteins such as vesicle associated membrane protein/synaptobrevin, synaptosomal-associated protein or syntaxin at neuromuscular junctions. Cleavages of SNARE proteins which are important in acetylcholine releasing, eventually leads to flaccid paralysis [13-16].

Nowadays, two kinds of vaccines are available for prevention of botulism toxicity, a multivalent vaccine for types A, B, C, D and E; and a monovalent vaccine for each types of A to G [17, 18]. Unfortunately, these vaccines are of limited accessibility all around the world and the risk of toxin reactivation of these vaccines is remained conflicting. Because of these limitations, recombinant vaccines are preferred as new vaccines [19]. The most common strategy for designing of botulism recombinant vaccine is based on the fragments of binding domain of neurotoxin serotypes which contains two dominant epitopes [20, 21]. One of the proposed recombinant vaccines which its proficiency as vaccine has been reported is an epitope-including fragment (93 residues) from C-terminus of botulinum neurotoxin type E ("recombinant botulinum neurotoxin type E heavy chain C terminal" or briefly "rBoNT/E-HCC") [22, 23].

Since producing a vaccine with least side effects is strongly desirable, vaccine producing industries attempt to develop oral vaccines which have several benefits such as mucosal immunity provoking, patient comfortableness and no need of highly qualified personnel for vaccination [24]. Although mucosal immunity of some BoNTs binding domain-based vaccine candidates was evaluated [19], there is no report regarding to mucosal immunity evaluation of rBoNT/E-HCC.

In our previous study we showed that rBoNT/E-HCC is able to provoke high titers of antibody in animal models when it is administrated intravenous [23]. Here, in aim of rBoNT/E-HCC evaluation as an oral vaccine, the effect of pH as the main factor in developing of oral vaccines was studied using different methods.

MATERIALS AND METHODS

Materials: All molecular biology grades chemicals and media for culturing the bacteria were obtained from Merck (Germany). Chemical agents for nickelnitrilotriacetic acid (Ni-NTA) resin were purchased from Qiagen (USA). LB (Lauria Bertani) powder was purchased from Difco (Sparks, MD, USA). The pET-contained *E.coli* strain was obtained from Agheli-Mansour, *et al*. [22].

rBoNT/E-HCC expression: The expression was performed as reported elsewhere [25]. Briefly the bacteria were cultured in LB broth, induced by 1 mM isopropyl-1-thio-□-D galactopyranoside (IPTG), and finally centrifuged (3200×g, 25°C, 6 min) to collect the

cells. 20 µl of cell lysate was loaded in 12% SDS-PAGE (sodium dodecyl sulfate-polyacrylamide) gel.

rBoNT/E-HCC Purification and Dialysis: As previously reported, purification of rBoNT/E-HCC as a polyhistidine tagged protein extract was done using a 50% Ni-NTA resin (NTA) with several washing buffers (C, D, E and MES buffers) [25]. The purified proteins electrophoresed on a 12% SDS-PAGE to confirm the purification. After protein purification, the rBoNT/E-HCC solutions were dialyzed in order to remove urea (8 M). For this purpose we used a dialysis bag that its cut-off-number was 12-KDa. After dialyzing, the protein samples were restored at -20˚C for following structural studies.

Fluorescence spectroscopy: In order to carry out intrinsic fluorescence experiments, a spectrofluorescence (Cary Eclipse Varian, Australia) which has a bath to control temperature was applied. 280 nm was applied as the excitation wavelength. The protein samples emission spectra were obtained at 300-500 nm in 10 nm bandwidth. The protein samples were at concentration of 0.1 mg/ml in buffer B (100 mM NaH_2PO_4, 10 mM Tris–HCl) at four pH values (2, 5, 7.4 and 9).

Circular dichroism (CD) spectropolarimetry: Circular dichroic spectra were obtained in far-UV regions (195-260nm) on a model J-810 Jasco spectropolarimeter at 25°C. The cuvette volume was approximately 0.5 ml, 1 millimeter path length. Concentration of the protein was 0.25 milligram per milliliter in buffer B (100 mM NaH_2PO_4, 10 mM Tris–HCl) and four different pH values (2, 5, 7.4 and 9). Protein secondary structures were taken using version 2.1.0.223 of CDNN program.

Aggregation: The aggregation of rBoNT/E-HCC (with concentration of 0.2 mg/ml in buffer B and four pH of 2, 5, 7.4 and 9) were studied by recording absorbance at 360 nm in a spectrophotometer (Cary-100 Bio VARIAN) by using of a quartz cuvette (with path length of 10 mm) [26]. Aggregation was studied by adding 50 mM dithiothreitol (DTT) to each sample to reduce disulphide bonds, as was described by Rudolph *et al.* [27]. Aggregation was continued for 180 min at 50°C.

RESULTS

rBoNT/E-HCC sequence: Figure 1 depicts rBoNT/E-HCC primary structure. The rBoNT/E-HCC contains the total of seventeen ionizable residues, six with negative charges (3 Asp and 3 Glu), eight with positive (2 Arg and 6 Lys), and three His which carry 3 positive charges at pH under 6. Considering these residues the net charge of protein at moderate pH is predominantly positive.

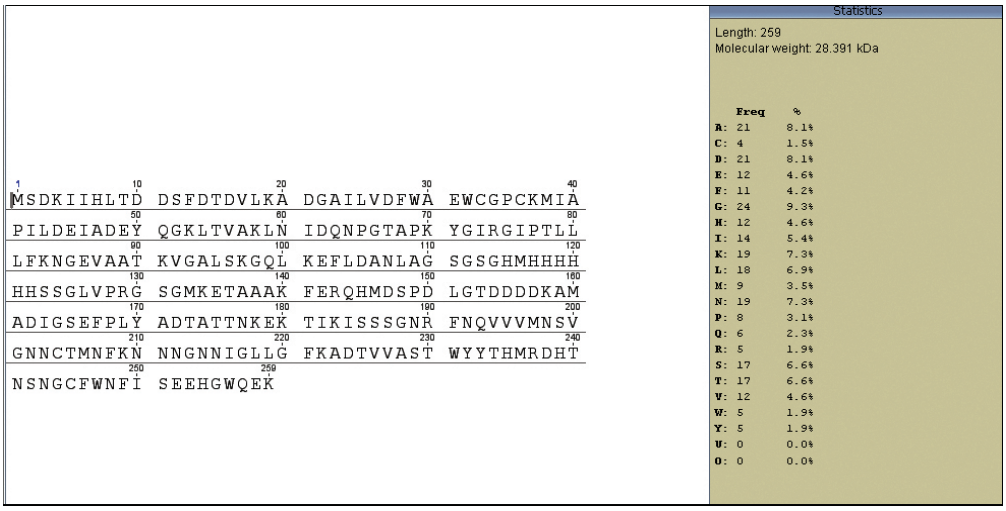

Figure 1: Complete sequence of rBoNT/E-HCC which is illustrated using Geneious R6 application.

Expression and purification of rBoNT/E-HCC*:* The rBoNT/E-HCC gene with a 6-His tag was utilized to express the recombinant protein. Each culture samples was tested for the presence of proteins using SDS polyacrylamide gel (12%) electrophoresis. The pET32a (+) system fused a ~ 18 KDa Trx family tag, containing 6-His tag to the gene [28]. Thus the final protein (Trx tag fused to 93 amino acid from C-terminal of botulinum neurotoxin type E), rBoNT/E-HCC, is expected to have a molecular weight of ~ 29 KDa. The rBoNT/E-HCC gene was highly expressed and the expression band was observed about 29 KDa (Figure 2-a). Purifying of rBoNT/E-HCC by Ni-NTA agarose column concluded a single band (~29 KDa), showing a highly purified protein, (Fig. 2-b). Our previous immunological study [23], introduced rBoNT/E-HCC (including it's His tag) as a vaccine candidate, so here we did not omit the His-tag to be able to link our results with the previous immunological result.

Fluorescence measurements: Fluorescence spectroscopy was used in structural study of rBoNT/E-HCC at different conditions. Figure 3 shows maximum emission of rBoNT/E-HCC at pH 2, 5, 7.4 and 9, at 349 nm with excitation wavelength of 280 nm. These emission patterns are characteristic of tryptophan residues (5 Trp of rBoNT/E-HCC) [29]. As it is depicted in figure 3, increasing the pH from 2 to 9 results in increasing of emission intensity directly. Considering the positive net charge of protein, the interpretation of the emission intensification seems to be easy. At pH 2 the protein takes a more compacted structure because of repulsive interactions between protein`s positive net charges and H^+ ions of buffer. The more compacted structure of rBoNT/E-HCC at acidic pH probably leads to quenching effects of other residues such as Arg or leads to more burial (less exposure) of Trp, result in preventing of attenuated emission producing [30]. Increasing the pH decreases the repulsive interactions between the protein and its environment, allowing rBoNT/E-HCC to take a more relaxed tertiary structure. These structural changes, increases the quantum of Trp exposure and ultimately causes hyperchromic effect.

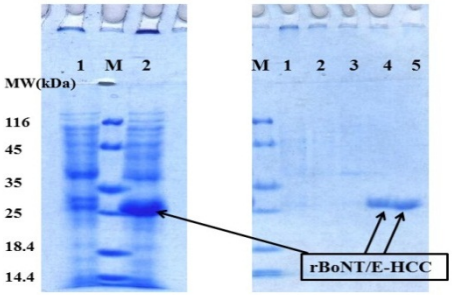

Figure 2: SDS-PAGE analysis of rBoNT/E-HCC expression in *E. coli* BL21 DE3. Columns 1 and 2 demonstrate cell lysate of *E. coli* BL21 DE3 containing pET32a before and after induction with IPTG respectively. Column M shows protein molecular weight marker. The expressed band was observed about 29-KDa. b) Purification of rBoNT/E-HCC on a Ni–NTA agarose affinity column. The separated protein fractions were run on 12% SDS–PAGE gel and stained with Coomassie blue stain. Column M, protein molecular weight marker; column 1, supernatant/soluble fraction after lysis of cells; column 2, wash buffer C (pH 6.9); column 3, wash buffer D (pH 5.9); column 4, wash buffer E (pH 4.5); column 5, 2-N Morpholino ethane sulfonic acid (MES) eluent. All C, D and E buffers have the same content (NaH_2PO_4 (100 mM), tris-base (10mM), Urea (8M)) whereas their pH is different. Purified rBoNT/E-HCC was obtained after adding E buffer and MES eluent.

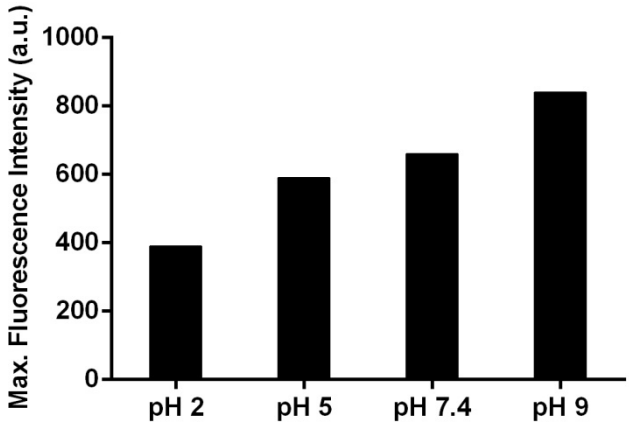

Figure 3: Fluorescence intensity of rBoNT/E-HCC solution in buffer B at pH 2, 5, 7.4 and 9 at 37°C. Increasing the pH from 2 to 9 amplify the emission intensity in a direct relation.

Circular dichroism and protein secondary structure: In order to investigate secondary structure alterations induced by different pH in rBoNT/E-HCC, circular dichroism spectra of the protein were obtained at pH 2, 5, 7.4 and 9. Figure 4 shows CD spectra of rBoNT/E-HCC and table 1 summarizes the corresponding secondary structures

obtained by spectral analysis using CDNN software, version 2.1.0.223. The results show that the major constituent of rBoNT/E-HCC secondary structure (>40%) is alpha helix. About 21% of residues take a random structure, which seem essential for protein flexibility in its native conformation. At pH 2 regular structures including alpha helix, beta structure (parallel and anti-parallel) and beta turn comprise 80 percent of protein residues. Increasing of pH led to decreasing of the regular structures. The random coil percent of rBoNT/E-HCC at pH 2 (21.31%) was changed to 26.27% and 28.08%, at pH 5 and 7.4 respectively, while the main regular structure, alpha helix, was changed from 56.27% at pH 2 to 46.95% and 43.74% at pH of 5 and 7.4 accordingly.

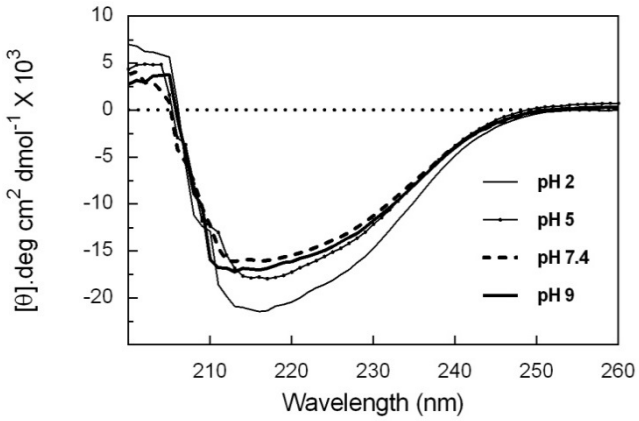

Figure 4: The far-UV CD spectra of the rBoNT/E-HCC at concentration of 0.25 mg/ml in buffer B (100 mM NaH_2PO_4, 10 mM Tris-HCl) at pH 2, 5, 7.4 and 9.

Table 1: The result of secondary structure analysis of rBoNT/E-HCC spectra (which are depicted in figure 4) by CDNN program, version 2.1.0.223.

	Percent of Secondary Structure				
pH	Helix	Beta-Sheet	Random Coil	Beta-Turn	Total
2	56.27	8.99	21.31	13.43	100
5	46.95	11.91	26.27	14.87	100
7.4	43.74	12.92	28.08	15.26	100
9	45.98	12.21	26.86	14.95	100

The pattern of secondary structures alterations from pH 7.4 to pH 9 seems to be unexpected; alpha helix amount was increased from 43.74% to 45.98% and random coil amount was decreased from 28.08% to 26.86%. If we assume that pH around 7.4 is isoelectric pH for rBoNT/E-HCC protein, the latest pattern may be interpreted. In such condition, it could be acceptable to expect that increasing pH from 7.4 to 9 decreases random coil structures and increases alpha helixes, although more studies should be done in this case. Furthermore the main difference is seen for pH 2 in which alpha helix

composes the major portion of the protein, and the slight differences between pH 5, 7.4 and 9 CD-pattern could be relinquished.

rBoNT/E-HCC Aggregation*:* thermal aggregation study of protein at 360 nm is a useful method to show the resistance of proteins to thermal denaturation. A thermal aggregation curve is composed of three phases, a lag phase, a logarithmic phase and a plateau phase [31, 32]. A large lag phase and a slow slope logarithmic phase indicate a more stable protein [32]. In order to simplify the aggregation experiment and prevent disulphide bond formation during experiment, which interferes with mechanisms involving in aggregation, we added 50 mM concentration of DTT to prevent disulphide bond formation. As it evident from Figure 5, the maximum rate of aggregation is seen in pH 9 and the lower rate for pH 2 which is in full agreement with this hypothesis that rBoNT/E-HCC has the more compacted and more stable structures at pH 2 and less stable structure at pH 9 [see ref. 30].

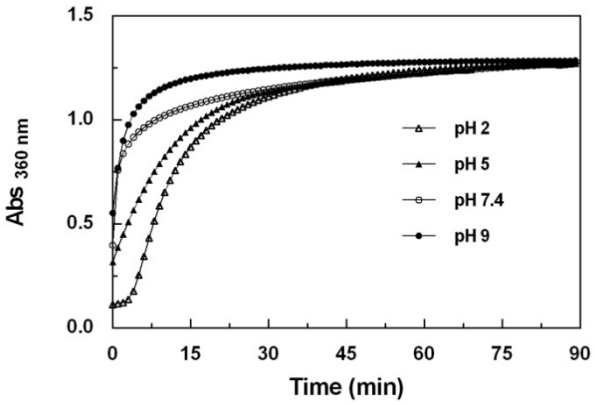

Figure 5: Thermal aggregation of rBoNT/E-HCC in the presence of 50 mM dithiothreitol for each sample. The more compacted and more stable structure of protein at pH 2 becomes more stable against thermal aggregation. Protein aggregation at pH 5, 7 and 9 increases with decrease in their stability accordingly.

DISCUSSION

In the present study different methods were used and their results were described according to the mechanism and the forces involved in each experiment. Fluorescence (Fig. 3) showed that increasing in pH from 2 to 9 expands protein from its compacted structure to slightly extended structure. CD studies showed that the protein tends to have more secondary structure at pH 2. Aggregation experiment (Fig. 5) indicated that rBoNT/E-HCC at 50°C aggregates in lower rate at pH 2. Altogether the results introduce a more compact and more stable form of rBoNT/E-HCC at acidic pH. It is noteworthy that observed structural difference on studied pH is not very extreme, so it is hard to judge

about the effect of these changes on the protein immunogenicity and more immunological studies are needed.

Although it seems that most proteins would be unfolded or partially folded at low pH, there may be an exception for Botulinum-based proteins, so that in the most relevant study to our finding, Bedu-addo *et al.* also indicated that optimal stability of rBoNTB(Hc) is seen at low pH [33].

Considering our results we can make a general conclusion as follow: i: exposure of rBoNT/E-HCC to different pH of 2, 5, 7.4 and 9 did not extremely change its secondary or tertiary structure (maximum change is about 6%). ii: It is thought that aggregation of proteins is undesirable in therapeutics use of protein [34]. Our results showed that rBoNT/E-HCC aggregation at physiological temperature of 37 ˚C is neglectable and in order to induce aggregation, 50°C is needed. iii) It seems that rBoNT/E-HCC is able to endure the harsh condition of gastrointestinal tract condition. It is stable at pH 2 (that is assumed as pH of stomach) and it also did not change extremely at alkaline pH that may consider as pH of other parts of gastrointestinal tract (intestine etc.).

Our finding as the first step of rBoNT/E-HCC structure evaluation, hopefully introduce it as a suitable vaccine candidate for oral administration, however we advise further studies on it in both biophysical and immunological point of view.

Acknowledgments

The authors wish to thank Imam Hussein Comprehensive University (Tehran, Iran) for financial support. We thank Dr. Seyed Latif Mousavi (Shahed University, Tehran, Iran) for providing pET32a-contained *E.coli*. The staffs of Institute of Biochemistry and Biophysics (IBB), University of Tehran, Iran, especially Prof. Moosavi-Movahedi and Mrs. Poursasan, are also acknowledged.

Conflict of Interest: Authors have no financial or any non-financial competing interests.

REFERENCE

1. Simpson LL. *Botulinum Neurotoxin and Tetanus Toxin*; Academic Press: San Diego CA 1989.
2. Hatheway CL. Toxigenic clostridia. Clin Microbiol Rev 1990;3:66-98.
3. Simpson LL. The origin, structure, and pharmacological activity of botulinum toxin. Pharmacol Rev 1981;33:155-188.
4. Maselli RA. Pathogenesis of human botulism. Ann N Y Acad Sci 1998;841:122-139.

5. Johnson EA, Goodnough MC. *Botulism*. In: *Topley and Wilson's microbiology and microbial infections: bacterial infections*; Coliter, L., Ballows, A., and Sussman, M., eds.; Arnold: London**,** 1998;3:723-741.
6. Dasgupta BR, Antharavally BS, Tepp W, Evenson ML. Botulinum neurotoxin types A, B, and E: fragmentations by autoproteolysis and other mechanisms including by O-phenanthroline-dithiothreitol, and association of the dinucleotides NAD(+)/NADH with the heavy chain of the three neurotoxins. Protein J 2005;24:337-368.
7. Ahmed SA, Byrne MP, Jensen M, Hines HB, Brueggemann E, Smith LA. Enzymatic autocatalysis of botulinum A neurotoxin light chain. J Protein Chem 2001;20:221-231.
8. Schiavo G, Montecucco C. Tetanus and botulism neurotoxins: isolation and assay. Meth Enzymol 1995;248:643-652.
9. Maruta T, Dolimbek BZ, Aoki KR, Steward LE, Atassi MZ. Mapping of the synaptosome-binding regions on the heavy chain of botulinum neurotoxin A by synthetic overlapping peptides encompassing the entire chain. Protein J 2004;23:539-552.
10. Tonello F, Morante S, Rossetto O, Schiavo G, Montecucco C. Tetanus and botulism neurotoxins: a novel group of zinc-endopeptidases. Adv Exp Med Biol 1996;389:251-260.
11. Cai S, Kukreja R, Shoesmith S, Chang TW, Singh BR. Botulinum neurotoxin light chain refolds at endosomal pH for its translocation. Protein J 2006;25:455-462.
12. Parikh S, Singh BR. Comparative membrane channel size and activity of botulinum neurotoxins A and E. Protein J 2007;26:19-28.
13. Schiavo G, Santucci A, Dasgupta BR, Mehta PP, Jontes J, Benfenati F, Wilson MC, Montecucco C. Botulinum neurotoxins serotypes A and E cleave SNAP-25 at distinct COOH-terminal peptide bonds. FEBS Lett 1993;335:99-103.
14. Schiavo G, Malizio C, Trimble WS, Polverino de Laureto P, Milan G, Sugiyama H, Johnson EA, Montecucco C. Botulinum G neurotoxin cleaves VAMP/synaptobrevin at a single Ala-Ala peptide bond. J Biol Chem 1994;269:20213-20216.
15. Blasi J, Chapman ER, Yamaski S, Binz T, Niemann H, Jahn R. Botulinum neurotoxin C1 blocks neurotransmitter release by means of cleaving HPC1/syntaxin. EMBO J 1993;12:4821-4828.
16. Ahmed SA, Olson MA, Ludivico ML, Gilsdorf J, Smith LA. Identification of residues surrounding the active site of type A botulinum neurotoxin important for substrate recognition and catalytic activity. Protein J 2008;27:151-162.
17. Middlebrook JL. Protection strategies against botulinum toxin. Adv Exp Med Biol 1995;383:93-98.
18. Robinson RF, Nahata MC. Management of botulism. Ann Pharmacother 2003;37:127-131.
19. Byrne MP, Smith LA. Development of vaccines for prevention of botulism. Biochimie 2000;82:955-966.
20. Kubota T, Watanabe T, Yokosawa N, Tsuzuki K, Indoh T, Moriishi K, Sanda K, Maki Y, Inoue K, Fujii N. Epitope regions in the heavy chain of *Clostridium botulinum* type E neurotoxin recognized by monoclonal antibodies. Appl Environ Microbiol 1997;63:1214-1218.

21. Atassi MZ, Dolimbek BZ. Mapping of the antibody-binding regions on the HN-domain (residues 449-859) of botulinum neurotoxin A with antitoxin antibodies from four host species. Full profile of the continuous antigenic regions of the H-chain of botulinum neurotoxin A. Protein J 2004;23:39-52.
22. Agheli-Mansour A, Mousavi SL, Rasooli I, Nazarian S, Amani J, Farhadi N. Cloning, high level expression and immunogenicity of 1163-1256 residues of C-terminal heavy chain of *C. botulinum* neurotoxin type E. Biologicals 2010;38:260-264.
23. Rostamian M, Mousavy SJ, Ebrahimi F, Ghadami SA, Sheibani N, Minaei ME, Arefpour Torabi MA. Comparative study of immunological and structural properties of two recombinant vaccine-candidates against Botulinum Neurotoxin type E. Iranian Biomed J 2012;16:185-192.
24. Mestecky J. The common mucosal immune system and current strategies for induction of immune response in external secretions. J Clin Immunol 1987;7:265-276.
25. Wingfield PT, Palmer I, Liang S. Folding and purification of insoluble (inclusion-body) proteins from *Escherichia coli*. Curr Protoc Protein Sci 2001;6:6.5.
26. Rezaei-Ghaleh N, Ramshini H, Ebrahim-Habibi A, Moosavi-Movahedi AA, Nemat-Gorgani M. Thermal aggregation of alpha-chymotrypsin: role of hydrophobic and electrostatic interactions. Biophys Chem 2008; 132:23-32.
27. Rudolph R, Bohm G, Lilie H, Jaenicke R. In *Protein Function. A Practical Approach*, edn 2. Edited by Creighton T.E. New York: IRL Press 1997.
28. LaVallie, ER, DiBlasio EA, Kovacic S, Grant KL, Schendel PF, McCoy JM. A thioredoxin gene fusion expression system that circumvents inclusion body formation in the *E. coli* cytoplasm. Biotechnology 1993;11:187-193.
29. Lakowicz JR. In: Principles of fluorescence spectroscopy*;* Springer: Berlin 2006: 3rd ed, Vol. 1, protein fluorescence chapter.
30. Ruddock LW, Hirst TR, Freedman RB. pH-dependence of the dithiol-oxidizing activity of DsbA (a periplasmic protein thiol:disulphide oxidoreductase) and protein disulphide-isomerase: studies with a novel simple peptide substrate. Biochem J 1996; 315:1001-1005.
31. Won CM, Molnar TE, McKean RE, Spenlehauer GA. Stabilizers against heat induced aggregation of RPR, 114849, an acidic fibroblast growth factor (aFGF). Int J Pharm 1998;167:25-36.
32. Wang W. Protein aggregation and its inhibition in biopharmaceutics. Int J Pharm 2005; 289:1-30.
33. Bedu-Addo FK, Johnson C, Jeyarajah S, Henderson I, Advant SJ. Use of biophysical characterization in preformulation development of a heavy-chain fragment of botulinum serotype B: evaluation of suitable purification process conditions. Pharm Res 2004;21:1353-1361.
34. Cromwell ME, Hilario E, Jacobson F. Protein aggregation and bioprocessing. AAPS J 2006;8:E572-E579.